

## Supplemental Information:

### Click Chemistry Stereolithography for Soft Robots that Self-Heal

T. J. Wallin<sup>1</sup>, J. H. Pikul<sup>2</sup>, S. Bodkhe<sup>3</sup>, B. N. Peele<sup>2</sup>, B. C. MacMurray<sup>1</sup>, D. Therriault<sup>3</sup>,  
B. W. Mcenerney<sup>4</sup>, R. P. Dillon<sup>4</sup>, E. P. Giannelis<sup>1</sup>, and R. F. Shepherd<sup>2\*</sup>

<sup>1</sup> Materials Science and Engineering, Cornell University, Ithaca, NY, USA

<sup>2</sup> Mechanical and Aerospace Engineering, Cornell University, Ithaca, NY, USA

<sup>3</sup> Department of Mechanical Engineering, Polytechnique Montreal, Montreal, QC; Canada

<sup>4</sup> Jet Propulsion Laboratory, Pasadena, CA; USA

#### Movie S1: Touchdown the Bear Being Manipulated

[https://www.dropbox.com/s/ayj23pmdfyqf53o/MovieS1\\_TouchdownTheBearManipulated.MOV?dl=0](https://www.dropbox.com/s/ayj23pmdfyqf53o/MovieS1_TouchdownTheBearManipulated.MOV?dl=0)

#### Movie S2: Cyclic Tensile Test

[https://www.dropbox.com/s/riop545a8bmj06t/MovieS2\\_CyclicTensileTest.mp4?dl=0](https://www.dropbox.com/s/riop545a8bmj06t/MovieS2_CyclicTensileTest.mp4?dl=0)

#### Movie S3: Kagome Tower Compression

[https://www.dropbox.com/s/ojmo20fqm6m451q/MovieS3\\_KagomeTowerCompression.mp4?dl=0](https://www.dropbox.com/s/ojmo20fqm6m451q/MovieS3_KagomeTowerCompression.mp4?dl=0)

#### Movie S4: Fluidic Elastomer Actuators at 2 psi

[https://www.dropbox.com/s/zyhsa6bn9lygoap/MovieS4\\_FEAs\\_2psi.mp4?dl=0](https://www.dropbox.com/s/zyhsa6bn9lygoap/MovieS4_FEAs_2psi.mp4?dl=0)

#### Movie S5: Autonomic Self-Healing of FEA

[https://www.dropbox.com/s/7w4k99kfshi98a0/MovieS5\\_Autonomic\\_SelfHealing.mp4?dl=0](https://www.dropbox.com/s/7w4k99kfshi98a0/MovieS5_Autonomic_SelfHealing.mp4?dl=0)

### Resiliency of the PMP Windows:

Qualitatively, we have been able to successfully use the same build window in the printer for 100s of hours, likely due to PMP's low surface tension, low swellability in common solvents, and chemical inertness. As we believe the primary mechanism for its success as a build window is low surface energy to promote delamination, we quantified the change in surface energy over time using goniometry, or contact angle measurements. We first performed these tests on a clean, unused sheet of PMP and then on a build window that has spent 100s of hours in use in our printers. Using 15  $\mu\text{L}$  drops of water, we measured (VGA Optima Contact Angle) the contact angle of the pristine PMP window to be  $98.15 \pm 7.38^\circ$  compared to  $95.95 \pm 4.57^\circ$  for the used build window. Fig S1 shows two representative droplets. The similar wettability of these two surfaces suggests that there is little fouling of the surface, and therefore little change in the surface energetics over this duration of use."

### Printed Resolution:

The resolution of a stereolithography resin is highly dependent on the printer used and parameters chosen. The Autodesk Ember printer project 1280 x 800 pixels on to a build area of 64 x 40 mm which yields a nominal x and y resolution of  $\sim 50$  microns. The photoradiation dosage, absorptivity of the resin and build stage translations combine to determine the z-axis resolution. For the printed synthetic muscle device shown in Fig. 4 of the main text, we used 5%6000 resin containing 1  $\text{mg mL}^{-1}$  of Sudan I, with a desired layer height of 100 microns and photoradiation dosage of  $w_e = 90 \text{ mJ cm}^{-2}$ . In Fig. 5, the 2.5%186 resin was utilized as the base material (with 1  $\text{mg mL}^{-1}$  Sudan I) and pressurizing fluid. Fig. S2 shows the surface of that monolithic device as measured 3D laser scanning microscope (Keyence VK-X260). Following the build direction (z-axis), the blue line displays a wave with an amplitude of  $\sim 50 \mu\text{m}$  and a period of roughly  $175 \mu\text{m}$ . The amplitude corresponds to the x and y resolution demonstrating that the 5%6000 resin reaches the nominal resolution of the projected pixel size. We infer z-axis resolution from the period which is well above the build stage translations of 100 microns in between printing steps. While some photopolymerization beyond the desired layer height might improve adhesion between adjacent layers, increasing the resin's absorptivity, or decreasing the photoradiation could enable greater z-axis resolution.

### Photo Differential Scanning Calorimetry:

Differential scanning calorimetry (DSCQ1000, TA instruments) was conducted under exposure to light. The sample and reference pans were left uncovered inside a modified cell with a dual light guide adapter. The cell was aligned such that the reference and sample pans received identical light intensity from the light source (Omnicure Series 1500, Lumen dynamics). As in the photorheology experiments, a filter was used ( $\lambda = 400\text{-}500\text{nm}$ ) and the power density was measured to be  $E_e \sim 10 \text{ mW}\cdot\text{cm}^{-2}$ . Samples were equilibrated at  $30^\circ\text{C}$  for 2 minutes prior to exposure for 3 additional minutes with a flow rate of  $50\text{mL min}^{-1}$ . All

data was analyzed in TA Quantitative Analysis software. Normalized heat flow curves ( $\text{mW mol SH}^{-1}$  vs time), as shown in Fig. S4, were integrated over the exposure using a horizontal sigmoidal baseline and scaled relative to enthalpy of polymerization for thiol-ene reactions ( $60 \text{ kJ}\cdot\text{mol}^{-1}$ ) to obtain the total conversion. For the 2.5%186 and 5%186 resins, the molecular mobility of the shorter V.S. species leads to a slightly faster conversion rate for the first second of polymerization; however, the low molecular weight ultimately limits the final conversion to  $\sim 82\%$  likely due to a reduced probability that the chain is long enough for both vinyl end groups to reach thiol counterparts on other polymers. When the V.S. molecular weight increases, a higher conversion (i.e., 96% conversion for 2.5%6000) becomes obtainable.

### 3D Printing:

Files for the Kagome Tower, NSF Logo, and Stanford Bunny were obtained freely on the internet. A .obj file of Touchdown the Bear statue was obtained from artist Brian Caverly and modified using Meshmixer™ software. All other files were created using Solidworks™ software. Using Autodesk Print Studio™, each design was imported, modified, sliced into discrete photopatterns, and converted to a .tar.gz format. The exposure times used varied from 1-5 s depending on the resin composition and layer height. To reduce jamming, the separation slide velocity was set to 2 rpm. Autodesk Ember 3D printer was used to print all objects shown. We mixed Sudan I with toluene in the ratio of  $1 \text{ mg mL}^{-1}$  and added this absorptive species to the resins before printing to limit cure depth to the layer height and improve z-axis resolution. Fig. S5 shows that the printed photopolymer blend is optically translucent, but without the addition of Sudan I, the orange absorptive species, z-axis resolution is poor and layer heights are clearly visible.

### Fluidic Elastomer Actuator:

Fig. S6 shows a schematic of the monolithic synthetic muscle device composed of a pair of antagonistic fluidic elastomer actuators. Two three-way solenoid valves (Parker model 912-000001-031) connected each actuation chamber to both the ambient atmosphere and a pressurized air source at  $\sim 14 \text{ kPa}$ . Inlet connections to the 3D printed objects were sealed by Sil-Poxy™ (Smooth-On, Inc.) silicone adhesive to prevent leakage. Using an Arduino Uno to control each valve, the antagonistic pair of inflation chambers were alternatively pressurized for 250 ms and then depressurized (via venting to the atmosphere) for 250 ms. With this cycling frequency, the actuator achieved steady-state actuation rapidly, with little deviation from the periodic displacement after the initial 1-2 cycles. This stable periodic actuation lasted for  $>5,000$  inflation cycles with no noticeable decay. Periods of greater than 250 ms similarly achieved bidirectional actuation, but at cycle durations of 100 ms or lower no coherent motion was detected.

**Table S1: The composition of resins that yield a 1:1 stoichiometry between thiol and vinyl groups**

| M.S.<br>(MWT: 4000-6000) |                  | V.S.             |                  |
|--------------------------|------------------|------------------|------------------|
| Thiol Mole %             | Amount added (g) | Molecular Weight | Amount added (g) |
| 2-3%                     | 970              | 186              | 30               |
| 2-3%                     | 884              | 500              | 116              |
| 2-3%                     | 502              | 6000             | 498              |
| 2-3%                     | 260              | 17600            | 740              |
| 4-6%                     | 942              | 186              | 58               |
| 4-6%                     | 794              | 500              | 206              |
| 4-6%                     | 338              | 6000             | 662              |
| 4-6%                     | 152              | 17600            | 848              |
| 4-6%                     | 66               | 43000            | 934              |

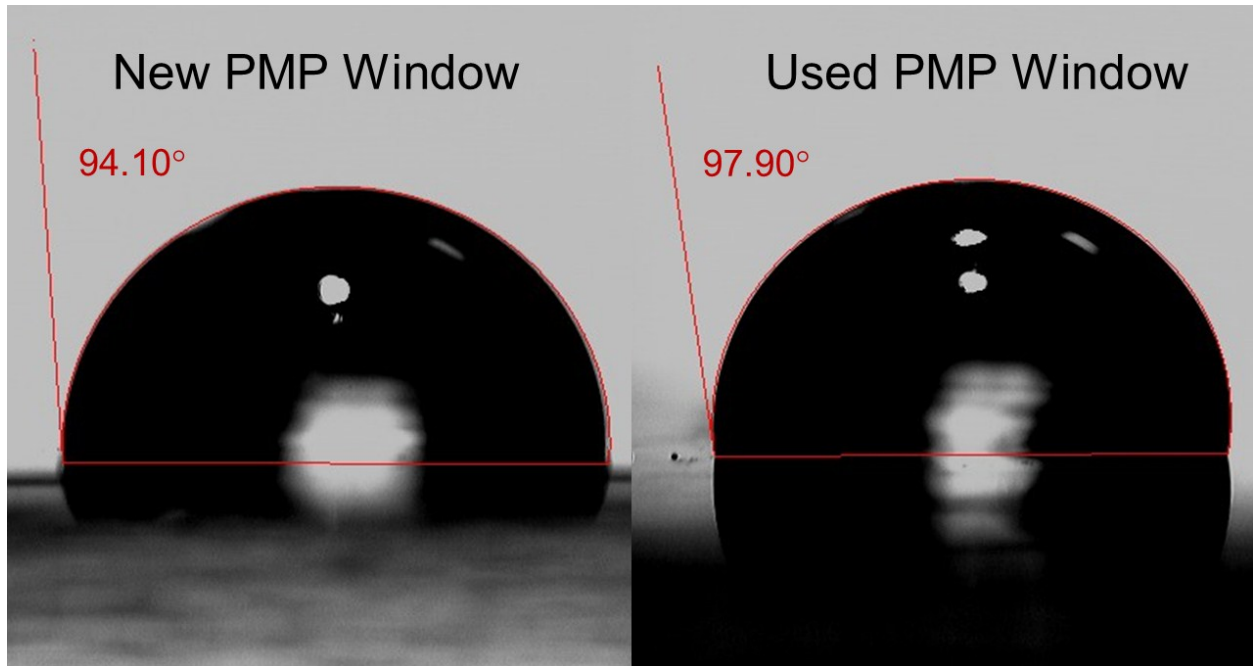


Fig. S1: The contact angle between water and PMP Windows before and after 100s of hours of use in the printer.

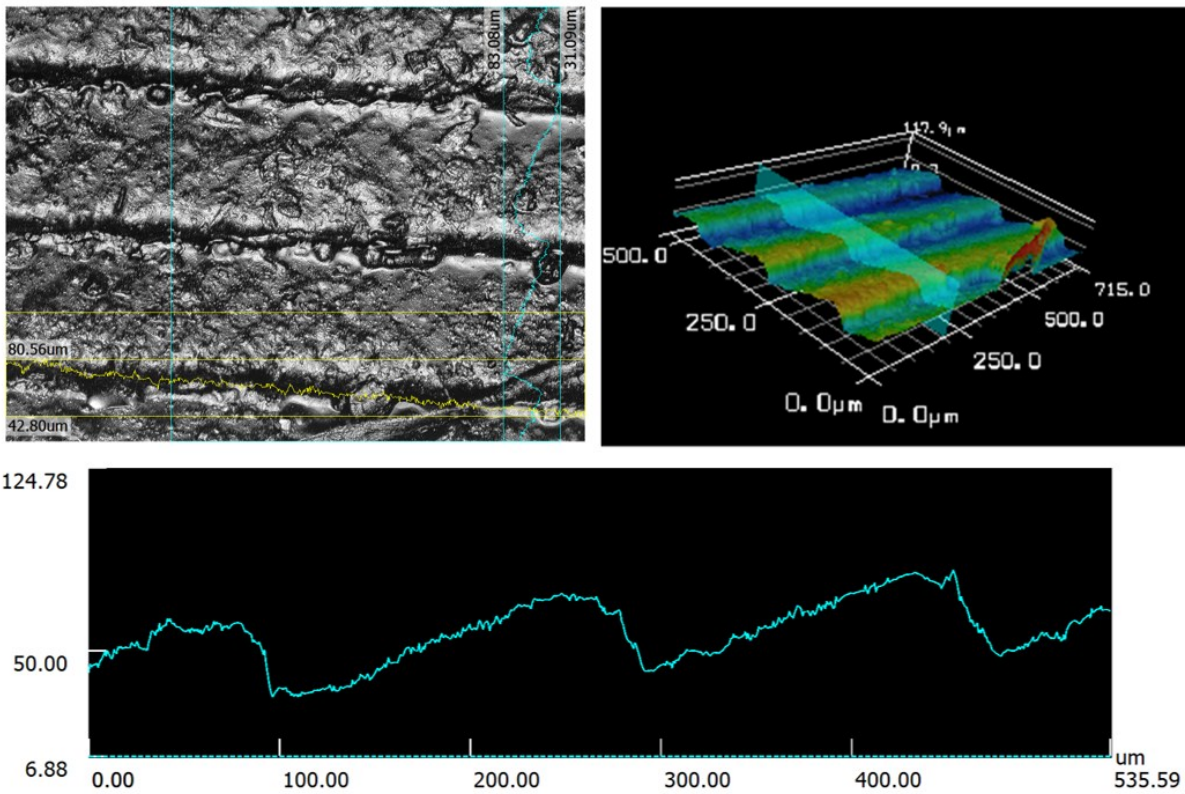


Fig. S2: 3D Laser Confocal Microscopy of Monolithic Device of Antagonistic FEAs. The blue line is parallel to build direction (z-axis).

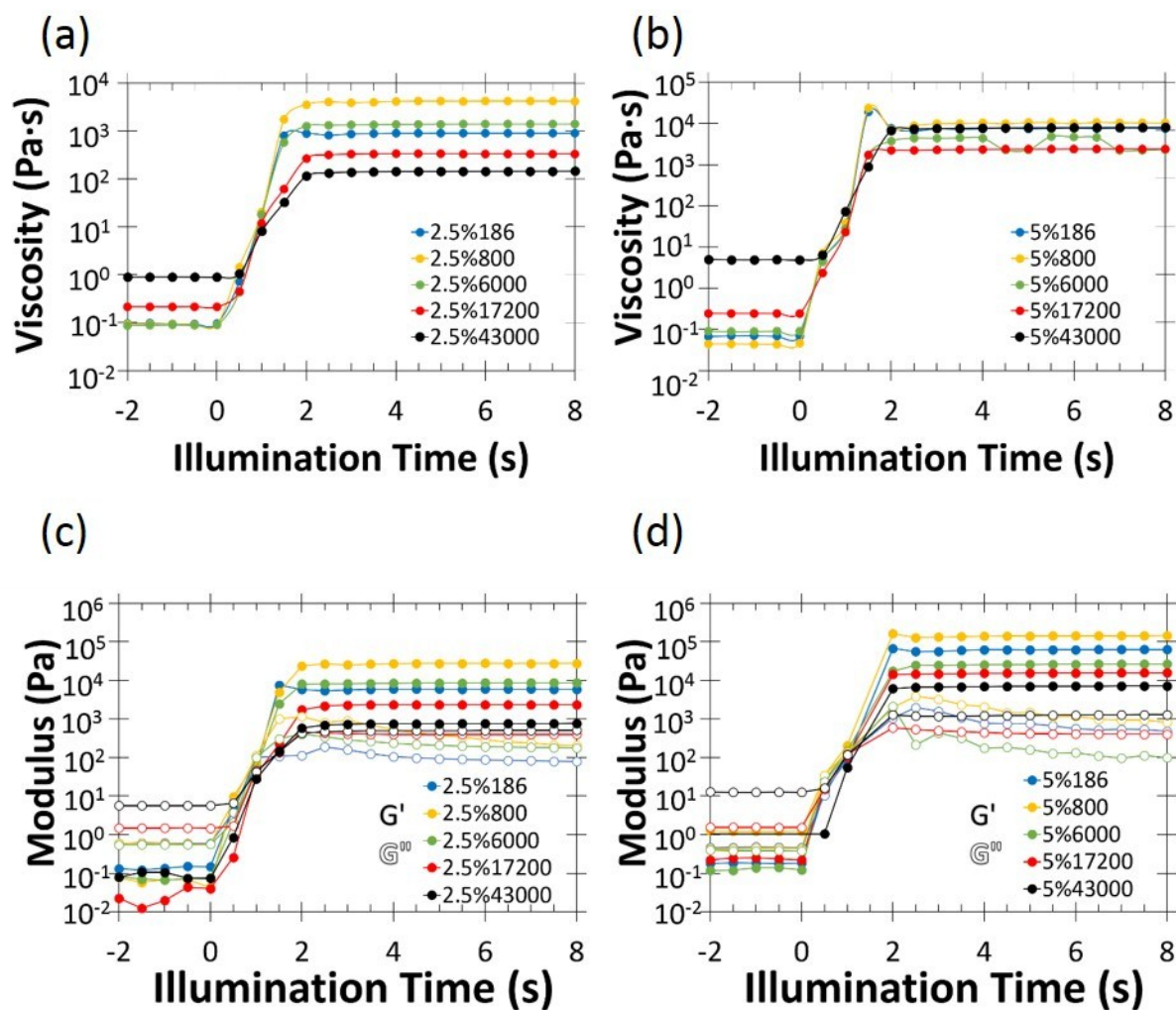


Fig. S3: Photopolymerization behavior for all resins. The time-evolution of the complex viscosity for resins based on (a) 2.5% and (b) 5% poly-mercaptopropylmethylsiloxane-co-dimethylsiloxane. The time evolution in the storage and loss moduli under photoexposure for (c) 2.5% and (d) 5% poly-mercaptopropylmethylsiloxane-co-dimethylsiloxane

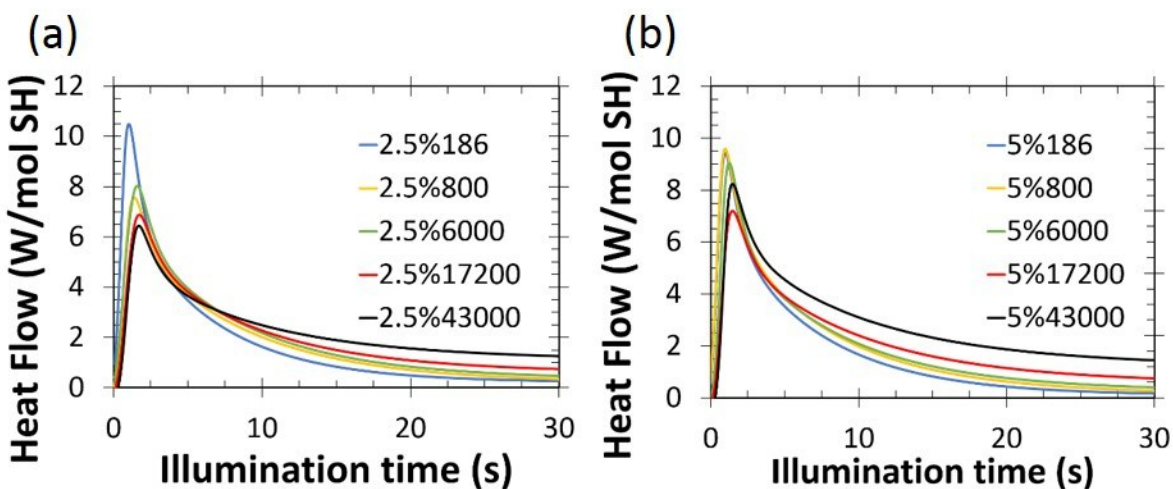


Fig. S4: Normalized heat flow vs. illumination time for the blends based on (a) 2.5% and (b) 5% poly-mercaptopropylmethylsiloxane-co-dimethylsiloxane

Table S2: Summarized photocure behavior for all blends.

| Sample Name | $t_{cure}$ (s) | $\eta_{t=0}$ (Pa.s) | $G'_{final}$ (Pa) | $G''_{final}$ (Pa) | Thiol Conversion (%) |
|-------------|----------------|---------------------|-------------------|--------------------|----------------------|
| 2.5%186     | <1.5           | 0.089               | 5600              | 62                 | 81.8                 |
| 2.5%800     | <1.5           | 0.088               | 24880             | 72                 | 85.8                 |
| 2.5%6000    | <1.5           | 0.089               | 8620              | 165                | 96.8                 |
| 2.5%17200   | <1.5           | 0.237               | 2310              | 410                | 83.0                 |
| 2.5%43000*  | <2.0           | 0.896               | 790               | 536                | 76.8                 |
| 5%186       | <1.0           | 0.057               | 31610             | 226                | 83.9                 |
| 5%800       | <1.0           | 0.044               | 62870             | 580                | 96.1                 |
| 5%6000      | <1.0           | 0.066               | 26890             | 91                 | 91.8                 |
| 5%17200     | <1.5           | 0.247               | 14850             | 42                 | 87.7                 |
| 5%43000     | <1.5           | 1.884               | 7430              | 1380               | 79.3                 |

The time to cure ( $t_{cure}$ ) is measured by the crossover in storage and loss moduli. The unreacted viscosity  $\eta_{t=0}$  was measured for 20 s prior to photoexposure.  $G'_{final}$  and  $G''_{final}$  are the stable values measured after 60 s of exposure. Similarly, Thiol conversion was calculated from the total enthalpy of polymerization after 60 s of exposure.

Table S3: Complete mechanical data for all blends

| Sample Name | Modulus $E$ (kPa) | Ultimate Elongation $\nu_{ult}$ (%) | Ultimate Stress $\sigma_{ult}$ (kPa) | Toughness (J m <sup>-3</sup> ) |
|-------------|-------------------|-------------------------------------|--------------------------------------|--------------------------------|
| 2.5%186     | 83 ± 11           | 110 ± 34                            | 64 ± 12                              | 26 ± 12                        |
| 2.5%800     | 56 ± 5            | 111 ± 22                            | 45 ± 8                               | 21 ± 7                         |
| 2.5%6000    | 19 ± 19           | 185 ± 29                            | 23 ± 4                               | 16 ± 2                         |
| 2.5%17200   | 6 ± 1             | 427 ± 49                            | 13 ± 3                               | 20 ± 10                        |
| 2.5%43000*  | *                 | *                                   | *                                    | *                              |
| 5%186       | 223 ± 19          | 48 ± 13                             | 88 ± 19                              | 32 ± 28                        |
| 5%800       | 287 ± 24          | 54 ± 13                             | 129 ± 20                             | 38 ± 16                        |
| 5%6000      | 85 ± 17           | 76 ± 15                             | 50 ± 12                              | 20 ± 8                         |
| 5%17200     | 32 ± 6            | 151 ± 8                             | 31 ± 7                               | 26 ± 8                         |
| 5%43000     | 9 ± 1             | 348 ± 32                            | 18 ± 4                               | 37 ± 11                        |

\*Sample 2.5%43000 was too soft to manipulate and so no measure mechanical properties were measured.

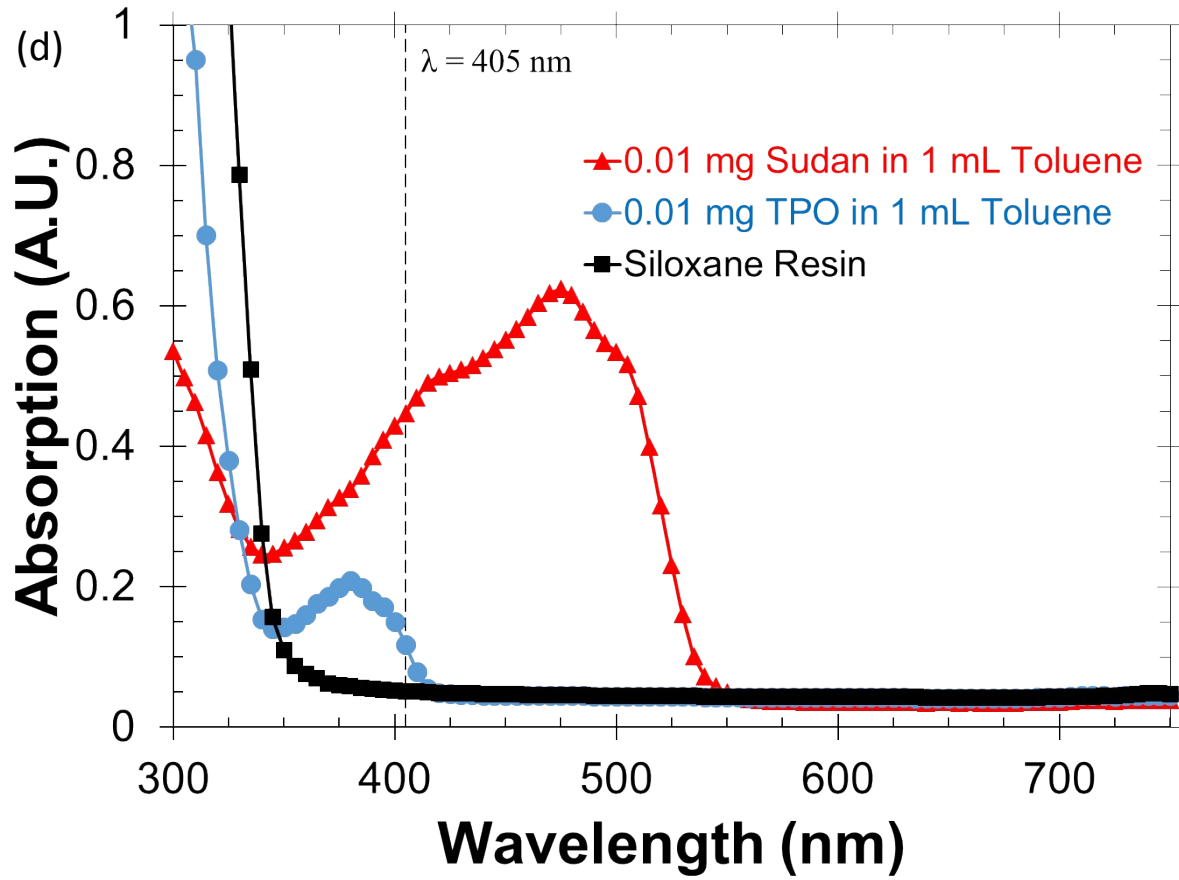
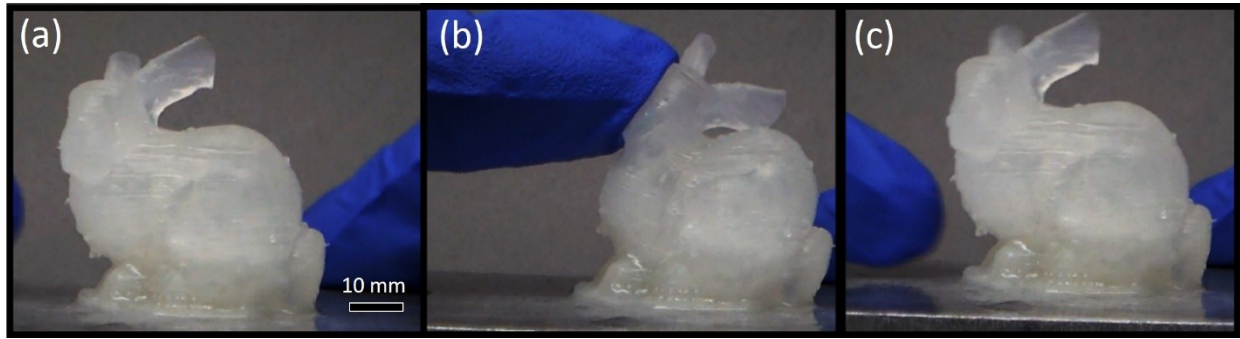
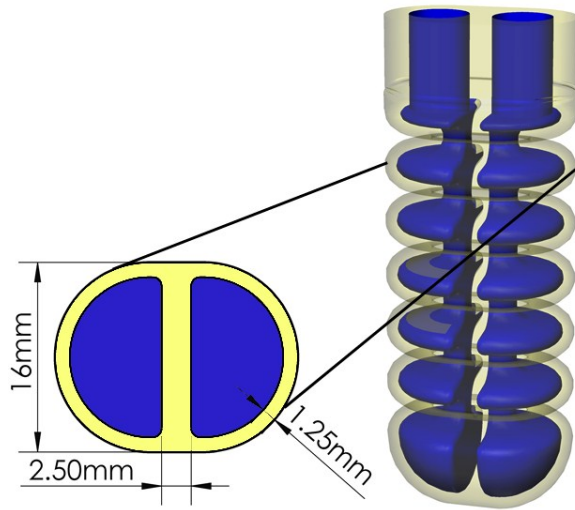


Fig. S5: A Stanford bunny model printed from 2.5%6000 material without incorporation of an absorptive species. This complaint structure is shown (a) before, (b) during, and (c) after manipulation and (d) the absorption of the individual components of our resin system





**Fig. S6: Schematic of Synthetic Antagonist Muscle Device.** Fluidic channels are colored blue, printed siloxane colore